# Time domain simulation of riser vibrations in current and irregular waves

J. V. Ulveseter, M. J. Thorsen, S. Sævik, C. M. Larsen

*7491 Trondheim, Norway, Department of Marine Technology, Norwegian University of Science and Technology*

**Abstract**

A semi-empirical time domain force model for combined cross-flow and in-line vortex-induced vibrations (VIV) is proposed, based on a series of earlier publications. The new feature is a term which represents the effect of vortex shedding in the flow direction, referred to as the in-line vortex shedding load. The latter is added to Morison's equation and a cross-flow vortex shedding force. The fundamental idea of how to model the effect of vortex shedding is the same as in previous works. An algorithm for synchronization is applied between the vortex shedding loading terms themselves and the structural response, which excites vibrations for a pre-determined frequency interval. The originality of the present study is rather how the VIV-terms are integrated as part of Morison's equation, which is there to provide a description of inertia and drag forces. All the loading terms combined enables simultaneous simulation of VIV and other response phenomena, such as wave induced motion and static drag displacement.

The performance of the time domain model is verified against measurements of a vertical riser subjected to two different external flow cases. The first one is simply steady uniform current whereas the second flow case combines the latter with irregular waves. To simulate the experiments, a linear finite element model of the riser is made, and the proposed hydrodynamic force model is applied to the translation degrees of freedom along the structure. It is to be noted that the same empirical coefficients are used to simulate both experiments. In uniform flow, the results are good. Dominating frequency and vibration amplitude agree well in both cross-flow and in-line directions. The simulated time series show more regular/less tendency of amplitude modulations than the experiments, but the overall agreement is still acceptable for engineering purposes. For the second flow case, where the riser was towed in irregular waves, the model provides a highly realistic representation of the riser motion. Both when the total response (containing wave and VIV frequencies) and the filtered signal (including only VIV frequencies) are analysed, the predictions follow the measurements closely. From before, the cross-flow part of the VIV model has been tested in oscillating flow and regular waves, and the performance of the former was experimentally proven. It is hence concluded that the proposed prediction tool is applicable to a variety of non-stationary flow conditions, implying that the synchronization model captures parts of the underlying physics, despite its simple form.

*Keywords:*
Vortex-induced vibrations (VIV), Irregular waves, Non-stationary flow, Time domain simulation, Semi-emprical model

## 1. Introduction

Bluff bodies exposed to fluid flow will experience flow separation leading to alternating vortex shedding in the wake if both Reynolds number (Re) and Keulegan-Carpenter number (KC) exceed certain thresholds [16]. If the structure is elastic, the oscillating lift and drag forces induced by the vortex shedding process can lead to structural vibrations, namely cross flow and in-line vortex-induced vibrations (VIV), respectively. Offshore engineering strongly rely upon the performance of elastic pipes, such as risers, umbilicals and pipelines, with bluff cross-sectional shapes, mostly circular. Such slender marine structures are exposed to ocean currents and waves, which makes VIV a concern both with respect to drag amplification an fatigue life.

Accurate prediction of VIV has turned out to be difficult due to the complex interaction between vortex shedding and structural response, which is reflected in the reviews by Sarpkaya [14] and Williamson and Govardhan [28], among others. This is why a substantial amount of researchers have performed experiments to improve our physical understanding of the phenomenon [25, 1, 3]. Measurements form the basis for what

is commonly referred to as semi-empirical VIV models, relying on empirical coefficients. VIVANA [12] and SHEAR7 [26] are two examples which are widely used in VIV assessment. Both programs solve the equation of motion in frequency domain, which limits analyses to linear structures and flows which are constant in time, i.e. stationary flows. Hence a time domain description of the hydrodynamic loading is desirable, where there are no such restrictions.

Previously published work on VIV in non-stationary flow is limited. This is probably because the more simple problem of a flexible cylinder in constant current is not yet fully understood. Non-stationary flow will increase the complexity as the cylinder now will face shed vortices upstream (instead of downstream) if the flow turns. Some experimental work has been carried out for rigid cylinders restricted to cross-flow motion in regular oscillatory flow [15] and in irregular oscillatory flow [9]. Quite recently, experiments were conducted with a flexible pipe in regular oscillatory flow [7] and for a Steel Catenary Riser (SCR) with prescribed heave induced motion at the riser top end [27]. Mo [11] conducted a test of a vertical riser towed with a constant speed in irregular waves.

Some examples are found where structural vibrations of cylinders exposed to non-stationary flows have been simulated and described. For instance, Thorsen et al. [18] used an earlier version of the cross-flow VIV model, which the present work is based upon, to simulate the experiments by Fu et al. [7]. The study showed good agreement with the measurements in terms of frequency, amplitude and mode. More recently, Thorsen et al. [19] was able to simulate the transverse vibrations of the SCR reported by Wang et al. [27], including non-linear effects such as the time varying seabed contact, in the analysis. Thorsen's latest work on cross-flow vortex-induced vibrations in non-stationary flow was published by Thorsen and Sævik [20], where a numerical study of a vertical riser subjected to harmonic waves was performed. However, no experimental validation was included in that work. This was also the case for a numerical study by Chang and Isherwood [4], where cross-flow VIV simulations of an SCR, vibrating due to vessel heave motion, was carried out. Here, two time domain prediction tools were compared, i.e. a vortex tracking (CFD) model and a wake oscillator model. It was concluded that the latter was less successful than the former, but that the wake oscillator might still be beneficial in preliminary studies. Solving Navier-Stokes equations through CFD is to prefer over semi-empirical methods because it provides insight into the actual flow characteristics. Additionally, the procedure is founded on fundamental theories, such as conservation of mass and momentum. A recent study of the cross-flow vibrations of an elastically mounted rigid cylinder in oscillatory flow was presented by Zhao et al. [29], using three-dimensional direct numerical simulation in combination with the equation of motion. However, the computational resources needed in such studies are, even for today's computers, substantial, which is why semi-empirical models still are beneficial. Liao [10] modelled VIV of a riser in unsteady-flow, and investigated the effect of non-dimensional parameters. Resvanis [13] compared the response of flexible pipes in steady and unsteady current, and proposed a non-dimensional parameter which divides the unsteady response into different regimes.

From the above literature review, it is clear that most work on VIV in time varying flow has focused on cross-flow vibrations, and that the time variability has been of harmonic nature. The present work aims to model simultaneous cross-flow and in-line vibrations of a flexible pipe exposed to a flow which displays stochastic time variations and has a non-uniform spatial distribution. More specifically, the flow is a combination of irregular waves and uniform current, where the latter velocity is varied systematically. Slender marine structures, in particular vertical risers extending above the free water surface, are commonly exposed to a combination of current and waves, making non-stationary flows of practical relevance. In modelling the dynamic behaviour under such environmental conditions, the state of the art engineering approach is to neglect VIV and use Morison's equation to model the hydrodynamic forces. Then, a separate fatigue evaluation due to VIV in stationary flow is conducted, and the accumulated damage for VIV is added to the damage produced by waves. The present study is a step towards a model where wave and current induced vibrations can be addressed simultaneously.

The subsequent numerical simulations are performed utilizing a semi-empirical time domain model, which has been in constant development since it was first proposed by Thorsen et al. [17]. Even though a combined cross-flow and in-line model was suggested by Thorsen et al. [21], the present work is the first publication, in this series of research, where the combined cross-flow and in-line VIV hydrodynamic force model is integrated as part of Morison's equation. The fundamental idea of the model relates to the communication between the vortex shedding forcing term in cross-flow (which is added to Morison's equation in the direction perpendicular to the instantaneous inflow felt by the cylinder), and the cylinder cross-flow response. For a frequency band

specified by the user, the cross-flow vortex shedding force is able to synchronize with the cylinder cross-flow velocity, and hence act as an excitation force. An in-line vortex shedding forcing term is added in the direction of the relative inflow velocity, and is restricted to vibrate with a frequency approximately two times that of the cross-flow vortex shedding force. Note that the frequency approximation is due to a synchronization model between the in-line vortex shedding force and the in-line response, which will be further addressed in section 3.

The rest of this paper is structured as follows: First, experiments by Mo [11] are presented, which later are used to demonstrate the capability of the proposed force model. Then, underlying assumptions, theory, flow description, and structural/numerical modelling are explained in some detail. Results from simulations are compared to measurements. They are discussed in terms of how well they agree and what physical effects are causing the response. The strain induced by different response phenomena (waves and VIV) are evaluated with respect to the fatigue design. At last, the behaviour of VIV in the case of uniform current alone versus the combined case of waves and current, is investigated.

## 2. Experiment

### *2.1. Description*

MARINTEK (now SINTEF Ocean) conducted experiments with a 10 m long vertical riser in their Towing Tank III, as part of the Norwegian Deepwater Programme (NDP). A description of the tests were reported by Mo [11], which is the basis for the following. Three flow conditions were experimentally simulated. The first case was towing with constant speed, i.e. uniform steady current, in still water, for a variety of velocities. The second case applied a similar towing procedure, but now irregular waves were generated in the towing tank. Two different seastates were tested. The last case included harmonic excitation of the upper end of the riser, for three different pairs of frequency and amplitude (not counting the case of a fixed upper end). The latter was performed in still water and in the irregular seastates, for several towing speeds.

In this paper, only the first and the second case are considered, and only one of the irregular seastates. The flow conditions and important structural properties of the two cases are summarized in table 1 and 2, respectively. A schematic illustration is provided in figure 1.

To measure the response, 10 accelerometers were positioned along the riser, on the inside, with roughly the same spacing between them. Due to water entrainment, number 1, 6 and 7 from bottom failed, and could hence not be included in the present study. For Case 1, measurements from the 10th accelerometer is also dropped, because the cross-flow accelerations were not stored on the data files. Wave probes were used in the wave measurements, to verify the properties of the seastate, i.e. significant wave heigh, peak period and zero up-crossing period.

Table 1: Flow properties of the two simulated cases [11]. Here, "-" symbolises "not applicable", since for Case 1, the riser was towed in still water.

| **Case** | **1** | **2** |
|---|---|---|
| Significant wave height ($H_s$) | - | 0.25 m |
| Peak period ($T_p$) | - | 2.45 s |
| Zero up-crossing period ($T_z$) | - | 1.74 s |
| Range of towing speeds ($U_c$) | 0.10 - 0.38 m/s | 0.12 - 0.28 m/s |

### *2.2. Post-processing of experimental data*

In order to compare numerical simulations with experimental results, useful information must be extracted from the acceleration measurements. First, a time window where the towing velocity had reached steady state, was manually chosen for each test run. The towing velocity $U_c$ was taken as the average value in this time interval. Then, the original unfiltered accelerations were transformed to the global cross-flow and in-line coordinate system, according to the orientation angles of the accelerometers reported by Mo [11]. The accelerations were Fourier transformed into the frequency domain and then converted back to time domain, as displacements. The displacements were subsequently band-pass filtered. The chosen frequency limits were not identical for the two cases. For flow case 1, where the towing was performed in still water, the lower

Table 2: Structural properties of vertical riser as reported by Mo [11]. Note that EI is calculated based on the assumption that Youngs modulus for rubber is 50MPa.

| **Parameter** | **Size** |
|---|---|
| Length (L) | 10.078 m |
| Diameter (D) | 0.023 m |
| Wall thickness (th) | 0.004 m |
| Bending stiffness (EI) | 0.56 $Nm^2$ |
| Pretension ($T_1$) | Case 1: 52.3 N. Case 2: 50.6 N |
| Pretension ($T_2$) | Case 1: 33.8 N. Case 2: 32.1 N |
| Mass per unit length | 0.576 kg/m |

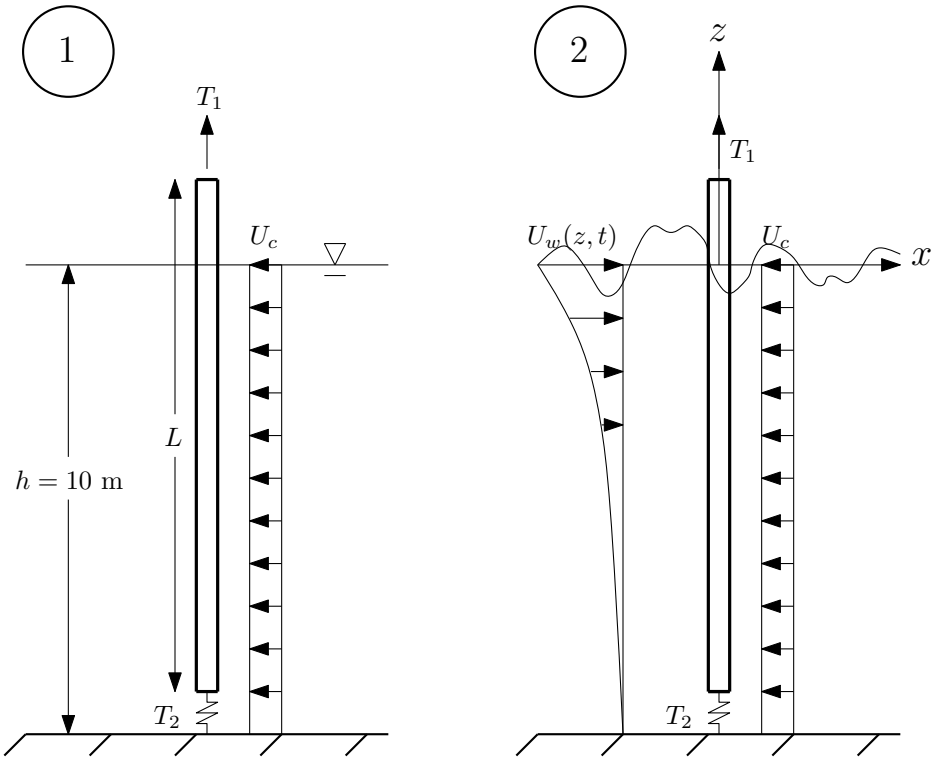


Figure 1: Schematic illustration of the experiments. Left: Uniform flow. Right: Uniform flow + irregular waves.

limit was taken to be the Strouhal frequency in the in-line direction, and half this value in cross-flow. The Strouhal number was chosen equal to 0.15, which is the same value as used by Mo [11]. The power spectra of the displacements were used to verify that, what was assumed to be VIV, was not filtered out (see the right plots of figure 6, 10 and 13). This was also the procedure when picking the higher frequency limit. For flow case 2, the response was separated into a component which included both wave and VIV frequencies, and one containing only VIV. In choosing the former, a lower limit of 0.3 Hz was used for all the relevant test runs, which was about 3/4 of the seastate peak frequency (recall table 1). For the displacement time series including the effect of VIV only, the high-pass limit was chosen a factor of 1.2 times the Strouhal frequency for the in-line vibrations. In cross-flow the same choice as for Case 1 was made, i.e. 0.5 times the Strouhal frequency. Again, the low-pass frequency limits were selected from visual inspection of the displacement power spectra.

A challenge when measuring response using accelerometers is to properly correct for their orientations, which might deviate from the global cross-flow and in-line directions. In the cross-sectional plane the average orientation angles were used to transform the time series to the global coordinate system, as stated above. However, as the riser vibrates, the accelerometers will also experience time varying orientations about the in-line and cross-flow axis. Since gravity is a conservative force which always points downwards, this has an

impact on the measurements, see e.g. Kaasen et al. [8]. The latter has not been accounted for in the present study, but the effect is not believed to be significant. As reported by Mo [11]:

> A change in riser orientation results in a change in the measured acceleration due to gravity. This effect has not been accounted for in the analysis. By analyzing the modal response time series, the size of the g-component is found to be in the range 0 - 8 % of the measure response.

## 3. Hydrodynamic loading model

The hydrodynamic force on a cylinder strip of unit length is given by:

$$\mathbf{F}_n = \underbrace{C_M \rho \frac{\pi D^2}{4} \dot{\mathbf{u}}_n - (C_M - 1)\rho \frac{\pi D^2}{4} \ddot{\mathbf{x}}_n + \frac{1}{2}\rho D C_D |\mathbf{v}_n| \mathbf{v}_n}_{\text{Morison's equation}} + \underbrace{\frac{1}{2}\rho D C_{v,y} |\mathbf{v}_n| (\mathbf{j}_3 \times \mathbf{v}_n) \cos\phi_{\text{exc,y}} + \frac{1}{2}\rho D C_{v,x} |\mathbf{v}_n| \mathbf{v}_n \cos\phi_{\text{exc,x}}}_{\text{Vortex shedding loading terms}}. \tag{1}$$

The three first terms are the well-known Morison's equation normal to the cylinder axis. It takes into account relative velocities and accelerations, i.e. the inflow felt by the cylinder as it moves. The external flow velocity vector is denoted $\mathbf{u}$, and the above dots symbolize time derivatives, meaning that $\dot{\mathbf{u}}$ is the external flow acceleration vector. The cylinder response is contained in the displacement vector $\mathbf{x}$, and the relative velocity normal to the cylinder axis is written $\mathbf{v}_n = \mathbf{u}_n - \dot{\mathbf{x}}_n$. The coordinate system and velocity vectors are illustrated in figure 2. $C_M$ and $C_D$ are the Morison's mass and drag coefficients, respectively. The two last terms of equation 1 are the vortex shedding loading terms in the instantaneous cross-flow and in-line directions, in that specified order. The instantaneous directions are determined from the direction of $\mathbf{v}_n$, which continuously changes as the cylinder vibrates. Hence, the cross-flow force component is directed perpendicular to the relative velocity, whereas the in-line component follows the direction of the Morison's drag force. $C_{v,y}$ and $C_{v,x}$ are the cross-flow and in-line vortex shedding force coefficients respectively, and $\phi_{\text{exc,y}}$ and $\phi_{\text{exc,x}}$ are the instantaneous phases of the vortex shedding forcing terms. $D$ is the cylinder diameter and $\rho$ is the seawater density.

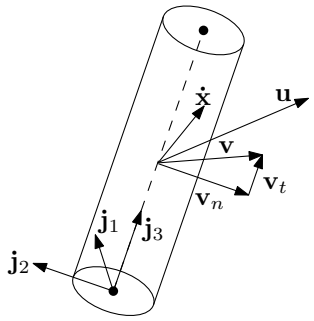


Figure 2: A cylinder segment with local coordinate system and velocity vectors [19].

To avoid potential misunderstandings in defining the cross-flow and in-line directions, and how the relative velocity $\mathbf{v}_n$ comes into play, study figure 3. It shows two cross-sectional cuts of the cylinder segment in figure 2. The left one illustrates the global definition of cross-flow and in-line, given by $y$ and $x$, respectively. It is defined from the direction of the undisturbed flow alone, i.e. $\mathbf{u}_n$. However, as structural vibrations develop, the relative inflow velocity $\mathbf{v}_n$ changes, which determines the directions of the vortex shedding forcing terms. From equation 1, these are given by:

$$\begin{aligned} \mathbf{F}_{v,x} &= \frac{1}{2}\rho D C_{v,x} |\mathbf{v}_n| \mathbf{v}_n \cos\phi_{\text{exc,x}} \\ \mathbf{F}_{v,y} &= \frac{1}{2}\rho D C_{v,y} |\mathbf{v}_n| (\mathbf{j}_3 \times \mathbf{v}_n) \cos\phi_{\text{exc,y}}. \end{aligned} \tag{2}$$

Even though the direction of $\mathbf{F}_{v,x}$ and $\mathbf{F}_{v,y}$ do not always coincide with the global $xy$-coordinate system, they are still referred to as the in-line and cross-flow vortex shedding force throughout this paper.

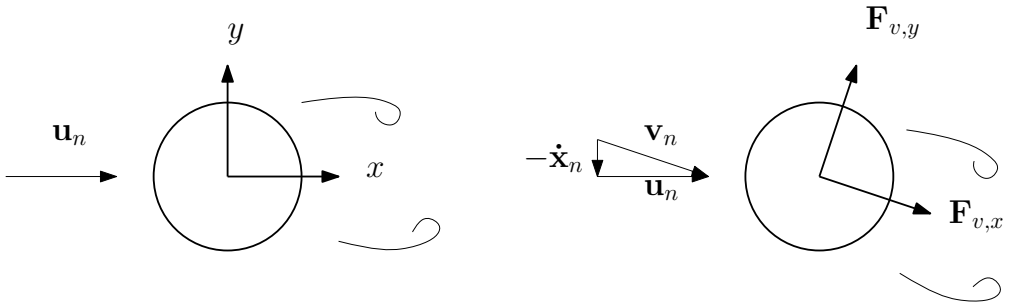


Figure 3: Left: Definition of in-line and cross-flow directions. Right: Directions of vortex shedding loading terms.

### *3.1. Cross-flow synchronization*

The vortex shedding frequency for a stationary cylinder is commonly expressed by the Strouhal relationship, i.e. $f_v = StU/D$, where $f_v$ is the vortex shedding frequency, $St$ is the Strouhal number, and $U$ is the undisturbed current velocity. In case of VIV, $f_v$ instead locks onto the cylinder oscillation frequency which coincides with its natural frequency when the actual added mass is accounted for. Then, resonance is achieved and the vibration amplitude transverse to the incoming flow is significantly amplified. Lock-in is represented by the instantaneous phase of the cross-flow vortex shedding force $\phi_{\mathrm{exc,y}}$, which, through a synchronization model, displays time variability depending on the cylinder response. For a limited band of non-dimensional frequencies, referred to as the synchronization range, the instantaneous frequency of the vortex shedding force is able to slow down or speed up to match the frequency at which the cylinder velocity vibrates. When synchronization is obtained, the vortex shedding force will act as an excitation force, transferring energy from the water to the structure. As the vibration amplitudes increase, damping from Morison's drag force will amplify, which ensures self-limiting vibrations. Outside the synchronization range, the vortex shedding force will unsuccessfully try to synchronize, providing a net energy input approximately equal to zero.

The instantaneous frequency of the cross-flow vortex shedding force is given by a differential equation:

$$\frac{d\phi_{\mathrm{exc,y}}}{dt} = 2\pi f_{\mathrm{exc,y}} = \frac{2\pi|\mathbf{v}_n|}{D}\hat{f}_{\mathrm{exc,y}}, \tag{3}$$

where

$$\hat{f}_{\mathrm{exc,y}} = \hat{f}_0 + \Delta\hat{f}\sin(\phi_{\dot{y}_{\mathrm{rel}}} - \phi_{\mathrm{exc,y}}). \tag{4}$$

The synchronization range is determined from $\hat{f}_0$ and $\Delta\hat{f}$, where the former represents the midpoint along the non-dimensional frequency axis, and the latter is the width. $\phi_{\dot{y}_{\mathrm{rel}}}$ is the instantaneous phase of the relative cross-flow velocity, which must be numerically approximated at every time step of a time domain simulation (see Thorsen et al. [19] for details). The cross-flow relative velocity of the cylinder response is written:

$$\dot{y}_{\mathrm{rel}} = \dot{\mathbf{x}} \cdot \frac{\mathbf{j}_3 \times \mathbf{v}_n}{|\mathbf{v}_n|}. \tag{5}$$

### *3.2. In-line synchronization*

In-line vortex-induced vibrations are typically separated into two branches. Pure in-line VIV takes place at low current speeds, when the vortex shedding frequency is lower than the first cross-flow eigenfrequency of the structure. Then, synchronization occurs for frequencies two or even three times the Strouhal frequency [16]. Pure in-line vibrations are not modelled here, since all the following case studies are outside of this regime. However, it is to be noted that a similar synchronization model as stated above has successfully been used for pure in-line vibrations [23, 24].

At higher current speeds, for bluff bodies free to move in all degrees of freedom, cross-flow induced in-line VIV may occur. Experiments, e.g. Dahl et al. [5], have shown that, in case of combined cross-flow and in-line

VIV, the latter vibrates with approximately two times the cross-flow frequency. These observations form the basis for the in-line synchronization model. According to Thorsen et al. [21], the instantaneous frequency of the in-line vortex shedding force is linked to the cross-flow component through:

$$\frac{d\phi_{\mathrm{exc,x}}}{dt} = 2\frac{d\phi_{\mathrm{exc,y}}}{dt}[1 + \alpha \sin(\phi_{\dot{x}_{\mathrm{rel}}} - \phi_{\mathrm{exc,x}})]. \tag{6}$$

Here, $\alpha$ is a factor that determines how far away from the double cross-flow frequency the in-line motion is allowed to travel. To fulfil the experimental observations, $\dot{\phi}_{\mathrm{exc,x}} \approx 2\dot{\phi}_{\mathrm{exc,y}}$, and so $\alpha << 1$. The other symbols in equation 6 express the equivalent in-line components of the ones stated in equation 4. The in-line relative velocity of the cylinder response is expressed as:

$$\dot{x}_{\mathrm{rel}} = \dot{\mathbf{x}} \cdot \frac{\mathbf{v}_n}{|\mathbf{v}_n|}. \tag{7}$$

## 4. Modelling of external flow in irregular waves

The undisturbed flow velocity, $U$, is one of the inputs to the hydrodynamic force model (since it is included in the expression of $\mathbf{v}_n$). In case of non-stationary external flow, the time and space variability of $U = U(z,t)$, must be represented. Here, $z$ is the vertical coordinate with origin at the mean free water surface (see figure 1) and $t$ is the time variable. The present work aims to model VIV of a vertical riser subjected to a combination of uniform current, $U_c$, and irregular waves, $U_w(z,t)$. Hence the total external flow velocity is written $U(z,t) = U_c + U_w(z,t)$. In the following, it is assumed that linear wave theory is valid up to the still water free surface, and that the horizontal wave particle profile alone can be used in simulating the waves. This means that the wave induced oval orbit of water particles is modelled only with its horizontal component, i.e. the vertical component is neglected. In addition, the cylinder diameter is assumed small compared to the wave height, so that diffraction can be disregarded. The riser motions are not taken into account in the wave modelling, meaning that wave particle velocities and accelerations are calculated at the static position of the riser.

Then, according to linear wave theory as reported by Faltinsen [6], the horizontal velocity profile of a regular wave with frequency $\omega_i$ and wave amplitude $\xi_{a,i}$, for a finite water depth $h$, is given by:

$$U_{w,i}(z,t) = \omega_i \xi_{a,i} \frac{\cosh(k_i(z+h))}{\sinh(k_i h)} \sin(\omega_i t), \tag{8}$$

and the horizontal acceleration profile by:

$$\dot{U}_{w,i}(z,t) = {\omega_i}^2 \xi_{a,i} \frac{\cosh(k_i(z+h))}{\sinh(k_i h)} \cos(\omega_i t). \tag{9}$$

The wave number $k_i$ is found from the dispersion relationship:

$$\frac{{\omega_i}^2}{g} = k_i \tanh(k_i h), \tag{10}$$

where $g$ is the gravitational acceleration. To convert from regular to irregular waves, superposition is utilized. Each wave component $i$ is given a uniformly distributed random phase angle between 0 and $2\pi$, which is named $\epsilon_i$. Hence, the total velocity and acceleration profiles become:

$$U_w(z,t) = \sum_i \omega_i \xi_{a,i} \frac{\cosh(k_i(z+h))}{\sinh(k_i h)} \sin(\omega_i t + \epsilon_i), \tag{11}$$

and

$$\dot{U}_w(z,t) = \sum_i {\omega_i}^2 \xi_{a,i} \frac{\cosh(k_i(z+h))}{\sinh(k_i h)} \cos(\omega_i t + \epsilon_i). \tag{12}$$

The acceleration profile is input to the first term of Morison's equation (recall equation 1).

The magnitude of the wave amplitudes, and how they distribute as function of wave frequency, depend on the seastate. In the experiment which the present work aims to simulate, the seastate is given by significant

wave height $H_s$, peak period $T_p$ and mean zero up-crossing period $T_z$ (recall table 1). Without any additional information about the irregular waves, it is assumed that the JONSWAP wave spectrum is applicable, and its peakedness parameter is chosen to be $\gamma = 3.0$. According to the 17th ITTC, the wave spectrum can be expressed as:

$$S_{\xi\xi}(\omega_i) = \frac{320{H_s}^2}{{T_p}^4}{\omega_i}^{-5}\exp(\frac{-1950{\omega_i}^{-4}}{T_p^4})\gamma^A \tag{13}$$

where:

- $A = \exp(-(\frac{\frac{\omega_i}{\omega_p}-1}{\sigma\sqrt{2}})^2)$
- $\omega_p = \frac{2\pi}{T_p}$
- $\sigma = 0.07$ if $\omega_i < \omega_p$
  $\sigma = 0.09$ if $\omega_i > \omega_p$

The amplitude of the individual wave components are given by:

$$\xi_{a,i} = \sqrt{2S_{\xi\xi}(\omega_i)\Delta\omega}, \tag{14}$$

where $\Delta\omega$ is the frequency interval when discretizing the spectrum.

To validate the above procedure, a realization of the wave elevation from linear wave theory, i.e. $\xi(t) = \sum_i \xi_{a,i}\sin(\omega_i t + \epsilon_i)$, is compared to what was measured by one of the wave probes. The result is presented in figure 4, and is found satisfactory. It should however be noted that the wave probe was installed on the carriage, meaning that the wave elevation is found relative to a coordinate system moving with the towing speed. Strictly speaking, since the total flow velocity $U(z,t)$ is applied to a riser assumed stationary, and because $T_p$ and $T_z$ reported in table 1 were planned according to a fixed coordinate system, the wave velocity and accelerations should be modified to account for the frequency of encounter. By Faltinsen [6], the encounter frequency is expressed as:

$$\omega_{e,i} = \omega_i + \frac{{\omega_i}^2 U_c}{g}\cos\beta, \tag{15}$$

where $\beta$ is the heading angle between the towing direction and the waves. Because the propagating speed of the wave profile, $c = g/\omega_i$, is significantly larger than the towing speed $U_c$, this effect is neglected in the present study.

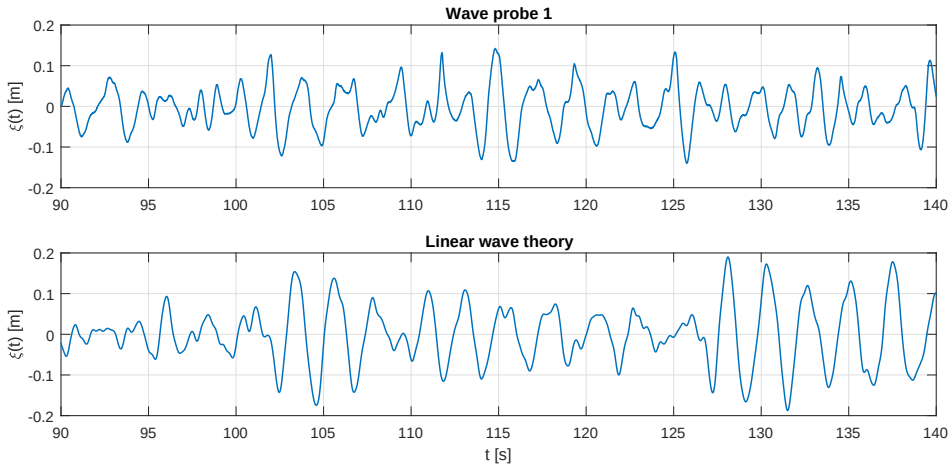


Figure 4: Upper: Wave elevation measured by the first wave probe for one of the test runs of Case 2. Lower: A realization of simulated wave elevation using linear wave theory and JONSWAP spectrum.

## 5. Numerical model and empirical parameters

A finite element model includes the global matrices for structural stiffness ($\mathbf{K}$), damping ($\mathbf{C}$) and mass ($\mathbf{M}$) of the riser. $\mathbf{K}$ accounts for bending stiffness and the pipe pretension. When towed, the riser will deflect due to mean drag forces, which in turn increases the tension forces above the values in table 2. Simulations verified that the displacement time series were not very sensitive to an increase of tension, which means that the results and discussions in section 6 are still representative of the experiment. The structural damping is assumed proportional to the stiffness matrix, i.e. $\mathbf{C} = \alpha_2 \mathbf{K}$, where $\alpha_2 = 10^{-4}$. For the range of dominating frequencies of Case 1 and 2, this choice implies a damping ratio of less than 0.1 % of critical. Standard linear beam elements, with two rotation and two translation degrees of freedom, have been used to describe the cross-flow and in-line motion, separately. Hence, the total response is found as the solution of an equation set, which is coupled through the hydrodynamic force model (recall the dependency on $\mathbf{v}_n$ from section 3). The dynamic equilibrium equation is expressed as:

$$\begin{aligned} \mathbf{M}\ddot{\mathbf{r}}_x + \mathbf{C}\dot{\mathbf{r}}_x + \mathbf{K}\mathbf{r}_x &= \mathbf{Q}_x \\ \mathbf{M}\ddot{\mathbf{r}}_y + \mathbf{C}\dot{\mathbf{r}}_y + \mathbf{K}\mathbf{r}_y &= \mathbf{Q}_y \end{aligned} \tag{16}$$

where,

- $\mathbf{r} = \{\mathbf{x}_1, \mathbf{x}_2, ..., \mathbf{x}_{ne}\}^T$ is the response vector at each node and $ne$ is the number of nodes.
- $\mathbf{r}_x = \{\mathbf{x}_{1,x}, \mathbf{x}_{2,x}, ..., \mathbf{x}_{ne,x}\}^T$ is the global in-line decomposition of the response vector.
- $\mathbf{r}_y = \{\mathbf{x}_{1,y}, \mathbf{x}_{2,y}, ..., \mathbf{x}_{ne,y}\}^T$ is the global cross-flow decomposition of the response vector.
- $\mathbf{Q} = \{\mathbf{F}_{n,1}l, \mathbf{F}_{n,2}l, ..., \mathbf{F}_{n,ne}l\}^T$ is the force vector at each node and $l$ is the element length.
- $\mathbf{Q}_x$ is the global in-line decomposition of the hydrodynamic force vector.
- $\mathbf{Q}_y$ is the global cross-flow decomposition of the hydrodynamic force vector.

The riser response is found by solving equation 16 with numerical time integration. Newmark-$\beta$, with parameters $\gamma = 0.5$ and $\beta = 0.25$ was applied. The time step was chosen so that each period of the cross-flow motion approximately contained 200 data points. The cross-flow frequency was approximated by the Strouhal frequency, i.e. $0.15U_c/D$, and it is emphasized that this approximation is only relevant for quantifying the time step. 200 such periods were simulated, and the 100 first were removed prior to post-processing. 300 elements were found acceptable with respect to convergence.

The Morison's drag and mass coefficients are chosen based on typical values of stationary circular cylinders in the sub-critical flow regime, i.e. $C_D = 1.2$ and $C_M = 2$. The cross-flow vortex shedding force coefficient is taken to be $C_{v,y} = 0.85$, which is lower than the default value proposed for the pure cross-flow model, but reasonable for such low Reynolds number [19]. The in-line vortex shedding force coefficient is $C_{v,x} = 0.8$, which is the same value as used by Ulveseter and Sævik [24], for pure in-line vibrations. Default values of the cross-flow synchronization range are utilized, i.e. $\hat{f}_0 = 0.18$ and $\Delta\hat{f} = 0.08$. The in-line frequency parameter, $\alpha$, is set to 0.15, which is similar to the study by Thorsen et al. [22]. The above information is summarized in table 3, and it is emphasized that the same empirical parameters have been used to simulate both flow cases.

## 6. Results and discussions

In this section, the numerical results and the post-processed experimental data, are compared. Before the model performance is discussed, the figure notations are explained.

Table 3: Empirical parameters in hydrodynamic force model used to simulate Case 1 and 2

| Parameter | Size |
|---|---|
| $C_D$ | 1.2 |
| $C_M$ | 2 |
| $C_{v,y}$ | 0.85 |
| $C_{v,x}$ | 0.8 |
| $\hat{f}_0$ | 0.18 |
| $\Delta\hat{f}$ | 0.08 |
| $\alpha$ | 0.15 |

### *6.1. Figure notations*

$x$ and $y$ symbolise the in-line and cross-flow displacement, respectively. When a single figure contains both these quantities, $A$ is the symbol which replaces $x$ and $y$ (figure 5, 9 and 12). As a measure of the amplitude level over a certain time period, the root mean square (rms) has been found. The rms of a discrete signal $x = \{x_1, x_2, ...n_N\}$, containing $N$ data points, is given by:

$$x_{rms} = \sqrt{\frac{1}{N}\sum_{i=1}^{N} {x_i}^2}. \tag{17}$$

For the figures showing how different quantities vary along the riser length (figure 6, 10 and 13), the previously defined vertical coordinate $z$, with origin at the mean water surface, is shifted downwards. The new vertical coordinate is defined by:

$$Z = z + L_{sub} \tag{18}$$

where $L_{sub}$ denotes the submerged length of the riser. Hence $Z = 0$ is at the lower end of the riser. $S_{xx}(f)$ and $S_{yy}(f)$ are the in-line and cross-flow power spectra, respectively. Abbreviations used are:

- CF - cross-flow
- IL - in-line
- sim - simulated
- exp - experimental

### *6.2. Case 1: Uniform current*

The model performance is verified by plotting the dominating frequency and maximum rms value of amplitude, as function of the current velocity, in figure 5. The frequencies compare well with the experiments in both cross-flow and in-line directions. The amplitudes are also seen to match good in the direction of the current, but the transverse motion is somehow overpredicted by the model. However, as mentioned in section 2, the experimental data are limited to six discrete points along the riser, in contrast to the 300 finite elements in the calculation. It is hence likely that the largest value of amplitude rms along the test riser was slightly higher than the largest value found at these six positions.

The longitudinal distribution of rms value of amplitude is provided in figure 6, for three current velocities. In addition, the figure contains the displacement power spectra at the positions of maximum rms value. High and low frequency components are filtered out, which is displayed in red colour. The experimental frequency content is in general slightly more broad-banded than in the numerical simulations, with a smaller peak at the dominating frequency. Even though the longitudinal distribution of vibration amplitude does not match perfectly, the predictions are of same order of magnitude as the measurements.

The displacement time series normalized by the riser diameter, in both cross-flow and in-line, are shown in figure 7. The longitudinal position is the same as for the power spectra, i.e. maximum rms of amplitude, and results for the same three current velocities as presented in figure 6, are plotted. The in-line experimental time series contain a small but notable frequency component which coincide with the dominating cross-flow

frequency. This might be because the orientation of the accelerometers varied slightly during the towing tests, so that the experimental values reported here do not match the global in-line and cross-flow coordinate system, perfectly. The predictions represent the amplitude level quite accurately. However, the amplitude modulation seems to be quite regular, whereas the measured time series were of a more stochastic character. An explanation might be that regular patterns are induced by the hydrodynamic force vectors dependency on the relative velocity. In case of steady-state response, $\mathbf{v}_n$ might repeat itself in time (over a significantly larger period than the VIV period), causing these regular vibrations patterns observed in figure 7.

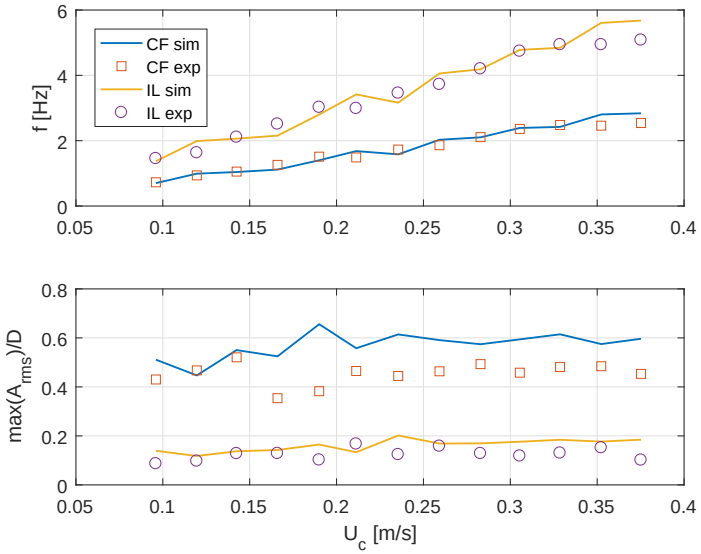


Figure 5: Upper: Dominating frequency as function of towing/current velocity. Lower: maximum rms of displacement amplitude normalized by the cylinder diameter as function of towing/current velocity. Case: Uniform current.

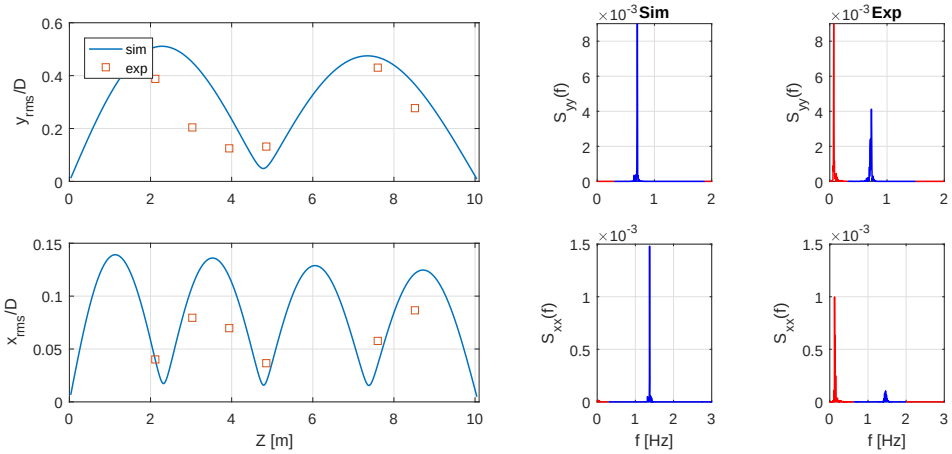


(a) $U_c = 0.096$ m/s

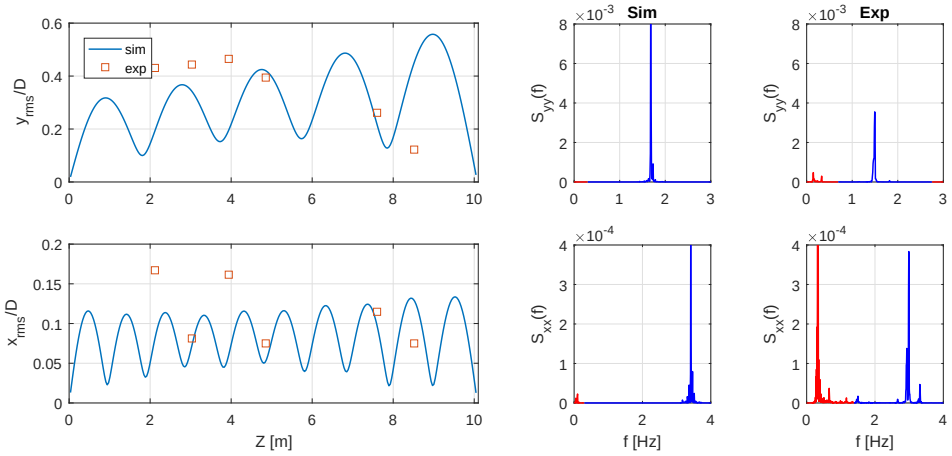


(b) $U_c = 0.211$ m/s

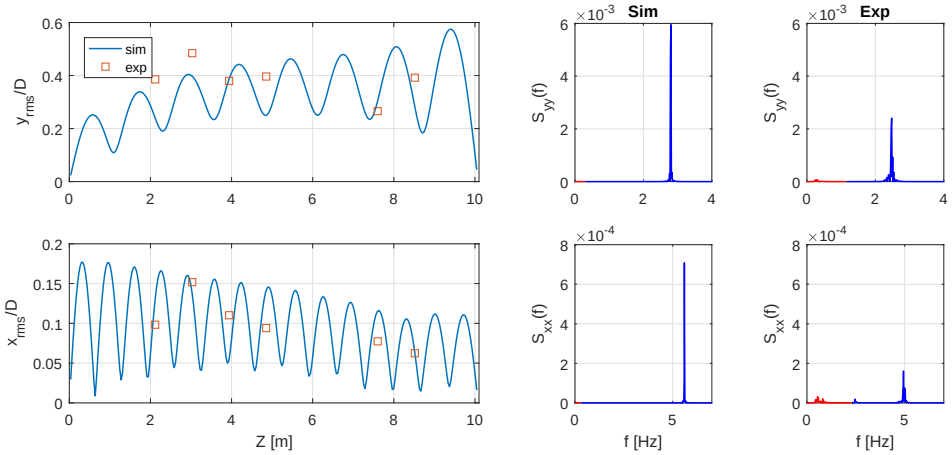


(c) $U_c = 0.352$ m/s

Figure 6: Left: Longitudinal distribution of non-dimensional displacement amplitude in terms of rms values. Right: Power spectral density of displacement at position of maximum rms value. The blue part of the power spectra illustrates the bandwidth which the presented results are based upon, and the red colour is the frequencies which have been filtered out. Case: Uniform current.

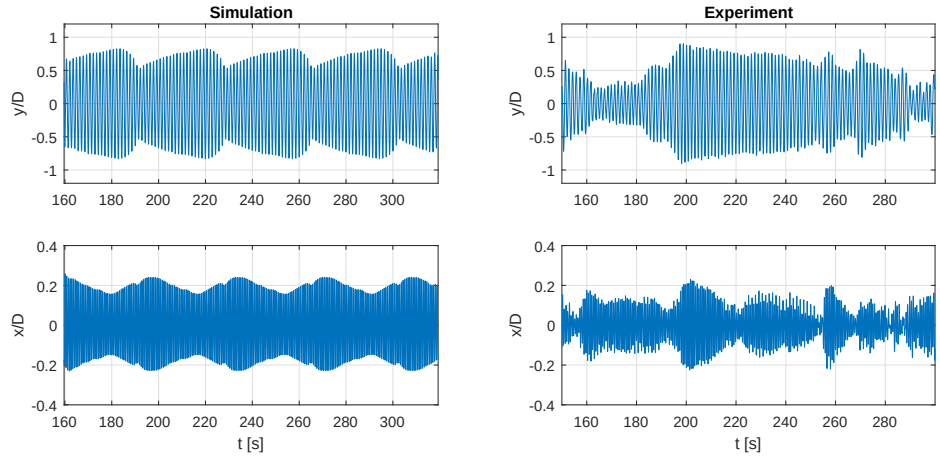


(a) $U_c = 0.096$ m/s

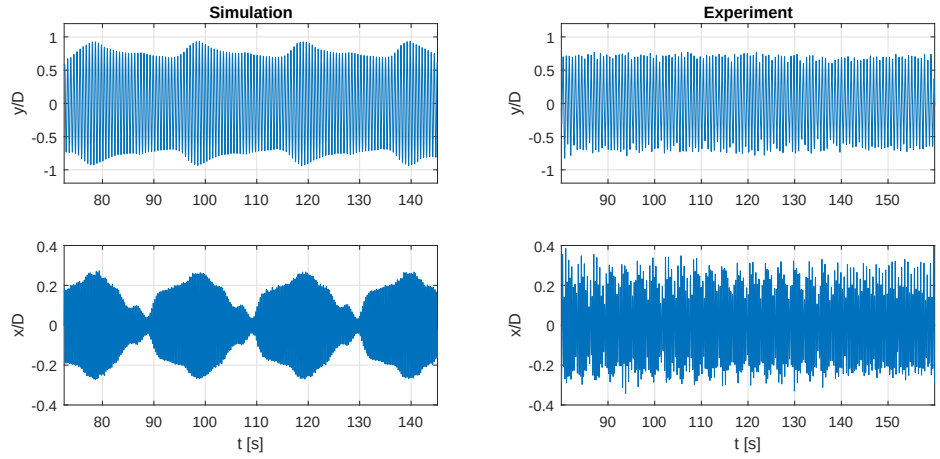


(b) $U_c = 0.211$ m/s

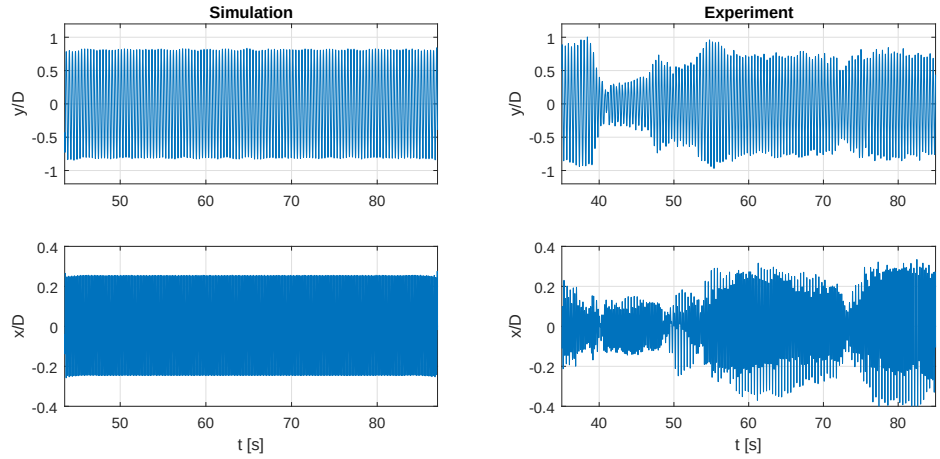


(c) $U_c = 0.352$ m/s

Figure 7: Normalized displacement time series at position of maximum rms of vibration amplitude. Case: Uniform current.

*6.3. Case 2: Irregular waves + uniform current*

For the second flow case, the results are split in two. The first part presents the total response containing the whole range of active frequencies (except for noise). The second part looks at VIV separately, by filtering out the low frequency components which are in range of the wave peak frequency.

The envelope of the undisturbed inflow along the riser length, and its time variation at two positions in the upper half of the pipe, are presented in figure 8. Three values of $U_c$ are considered, which are the same velocities used when the riser response is evaluated in the subsequent sections. Even for the lowest towing speed, where the wave particle velocity can vary with an amplitude about five times larger than $U_c$, most of the submerged part of the riser is dominated by current only. This is because the wave effect decreases rapidly with water depth, and so for $Z \in (0, 5)$ m, the envelope of $U = U_c + U_w$ more or less coincide with $U_c$. For $U_c = 0.119$ m/s and 0.212 m/s, the upper 2 m and 1 m of the riser, respectively, experience that the total inflow changes direction at certain time periods. For the highest current velocity, the total inflow is directed with the current more or less for the whole time window.

*Total response*

Dominating frequency and maximum rms of displacement amplitude are shown for a range of towing velocities between 0.12 m/s and 0.28 m/s, in figure 9. To illustrate the stochastic nature of the response, the envelope of results obtained from five realisations of the same seastate, is indicated by shadows. The line which is drawn through the envelope is the mean value of these five runs. Unlike the uniform current case, where the in-line vibrations oscillate with twice the cross-flow frequency, the wave frequencies now dominate the in-line motion, reducing the frequency to about 0.3-0.4 Hz. Since the seastate is identical for all towing speeds, the in-line frequency does not vary with $U_c$. The in-line displacement amplitudes are also dominated by the wave forces. In fact, they exceed the amplitude level of the cross-flow vibrations. It is interesting that the latter shows small changes compared to the case of current alone, both in terms of frequency and rms of amplitude. All these effects are, to a large degree, captured by the proposed model.

Both longitudinal distribution of vibration amplitude, and the displacement power spectra, match the experiments fairly accurate (see figure 10). The in-line power spectra contain a large peak at the wave frequency, and a smaller peak caused by VIV at a higher value. The VIV frequency increases as the current speed is raised. The simulated cross-flow response has become more broad-banded than for Case 1, which is a more realistic representation. Turning to the distribution of rms of amplitude, the in-line motion is largest at the top end of the riser, where the wave effect is significant. The vibration energy is transferred downwards to the lower end, as travelling waves. The cross-flow motion is less influenced by the waves, which explains that cross-flow amplitudes do not decay as much for increasing water depth.

Displacement time series are presented in figure 11. Transverse to the flow, the measured response looks slightly more chaotic than produced by the model. However, the simulations shown here should be regarded as a realization of a random process, since the waves are of a stochastic nature. Hence, other realizations might display higher amplitude modulation. It is difficult to distinguish between in-line time series from towing tests and simulations. The amplitude level, dominating frequency, and the high frequency component due to VIV, are all realistically modelled.

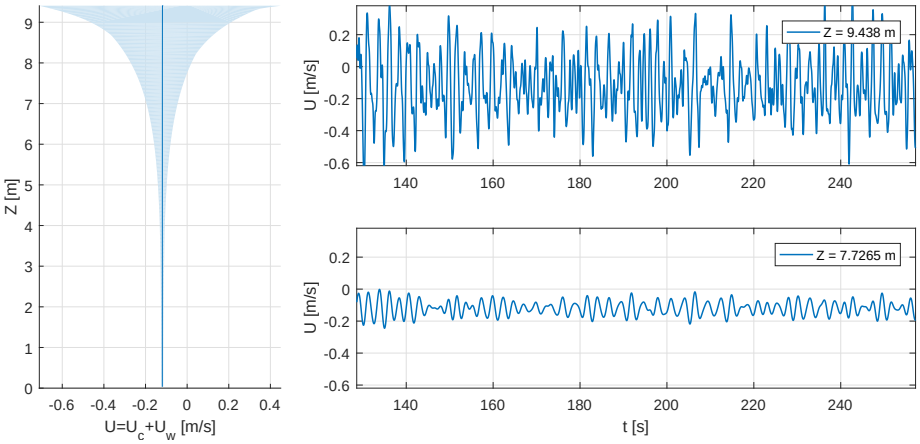


(a) $U_c = 0.119$ m/s

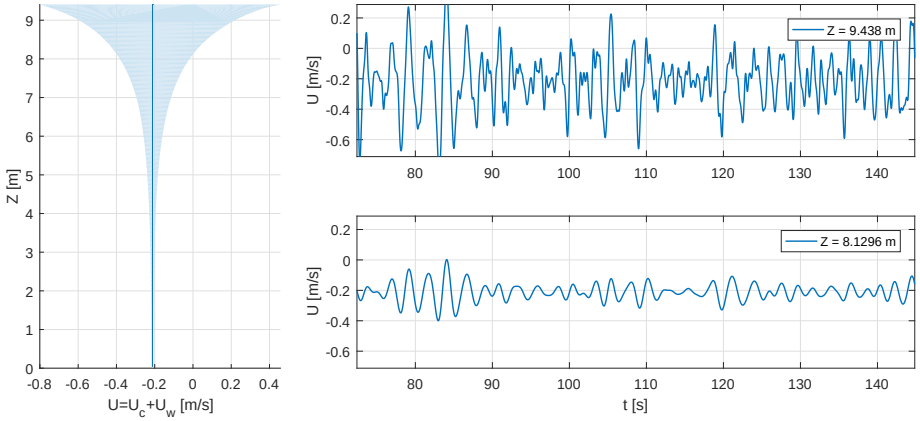


(b) $U_c = 0.212$ m/s

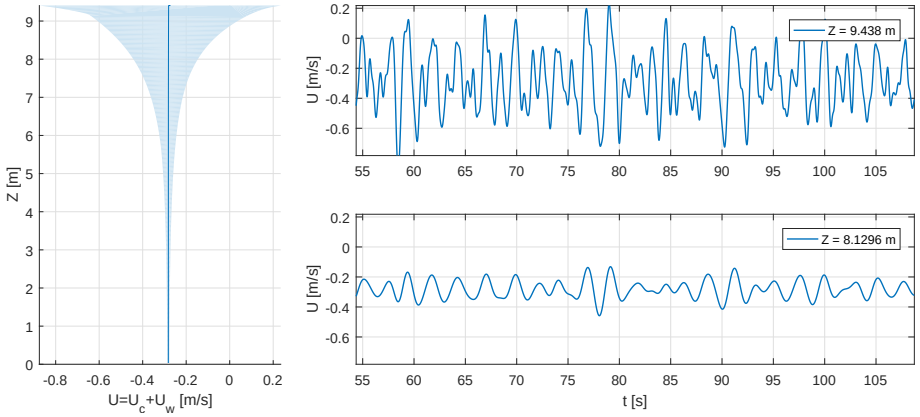


(c) $U_c = 0.282$ m/s

Figure 8: Left: Envelope of the total income velocity ($U = U_c + U_w$) from lower riser end up to the mean free surface. Right: Time series of $U$ at two longitudinal positions: At mean free surface ($Z = 9.438$ m), and at position of maximum in-line response.

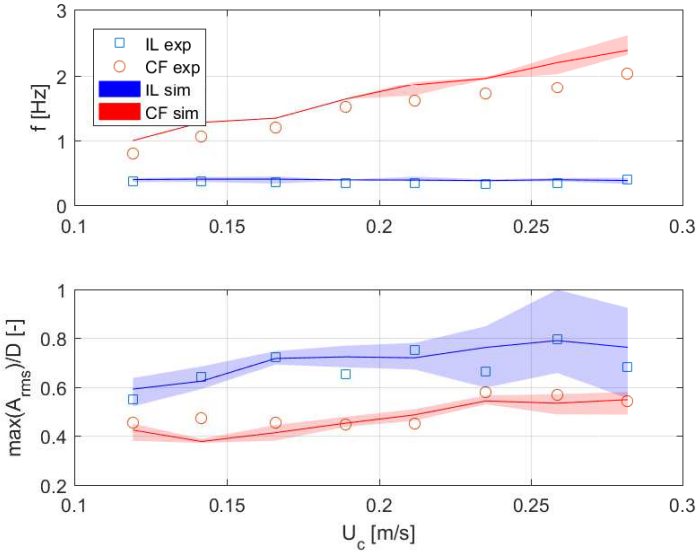


Figure 9: Upper: Dominating frequency as function of towing/current velocity. Lower: maximum rms of displacement amplitude normalized by the cylinder diameter as function of towing/current velocity. The stochastic response variation is illustrated by including envelops based on five simulations. Case: Irregular waves + uniform current.

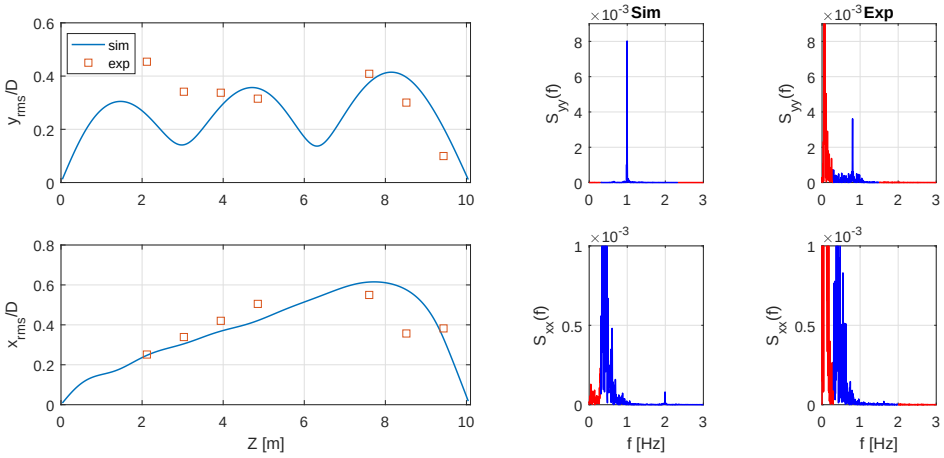


(a) $U_c = 0.119$ m/s

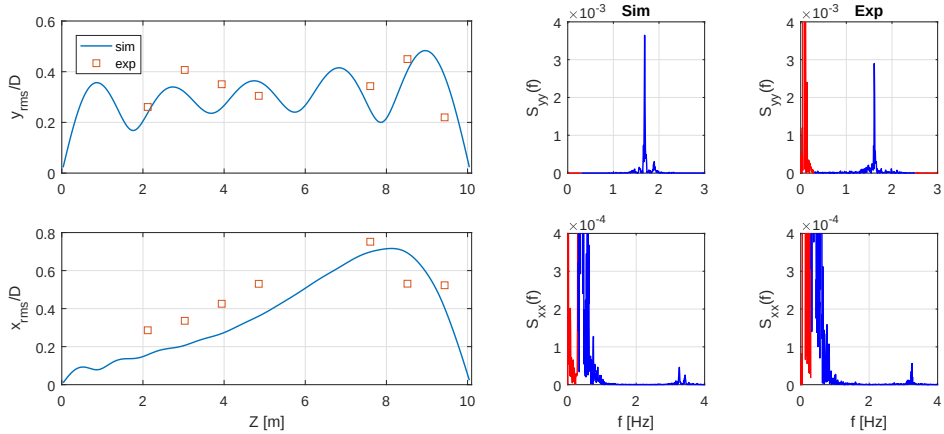


(b) $U_c = 0.212$ m/s

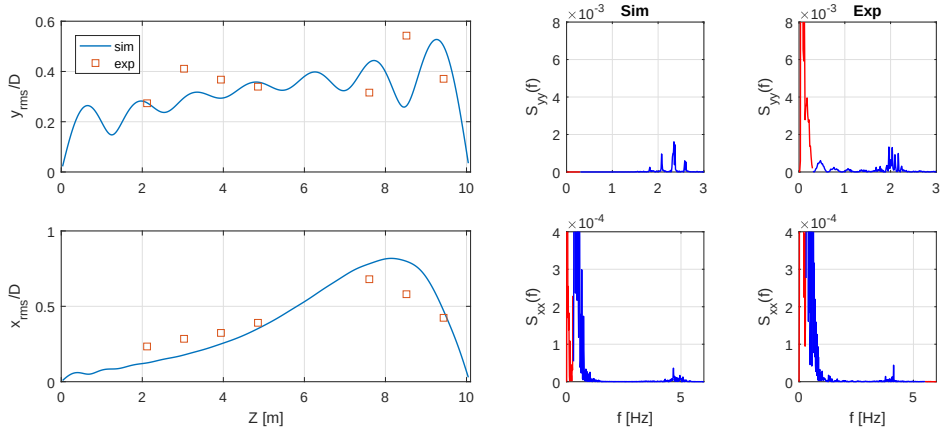


(c) $U_c = 0.282$ m/s

Figure 10: Left: Longitudinal distribution of non-dimensional displacement amplitude in terms of rms values. Right: Power spectral density of displacement at position of maximum rms value. The blue part of the power spectra illustrates the bandwidth which the presented results are based upon, and the red colour is the frequencies which have been filtered out. Case: Irregular waves + uniform current.

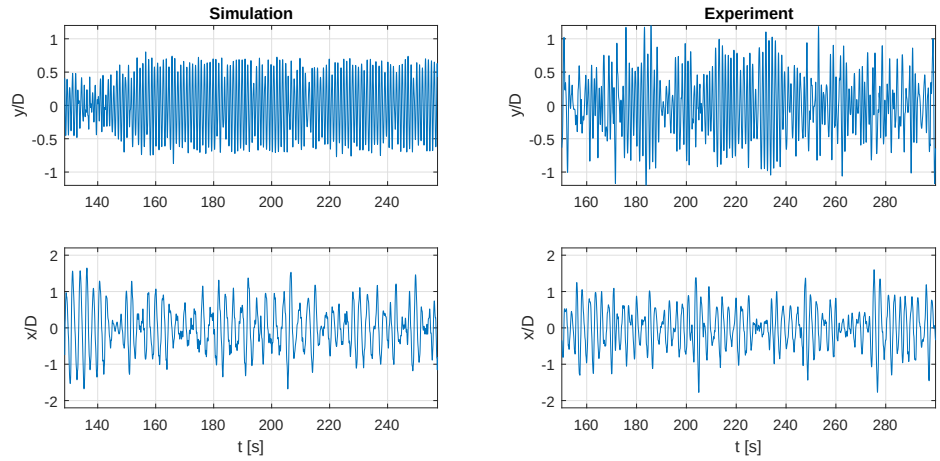


(a) $U_c = 0.119$ m/s

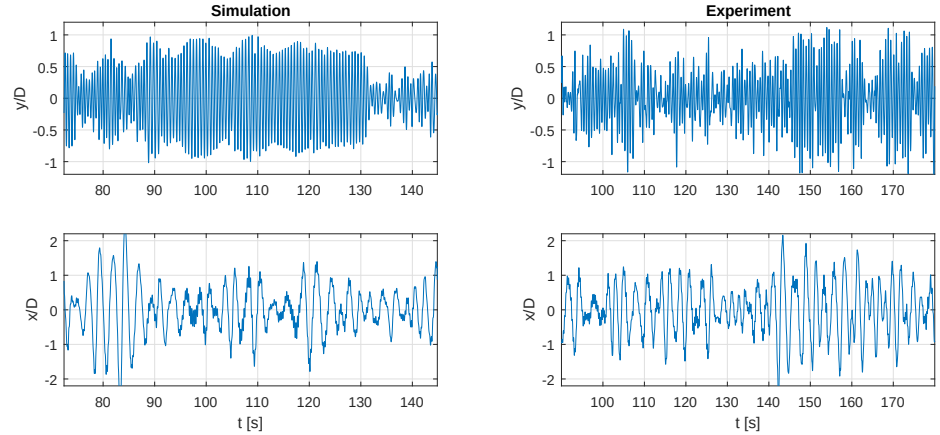


(b) $U_c = 0.212$ m/s

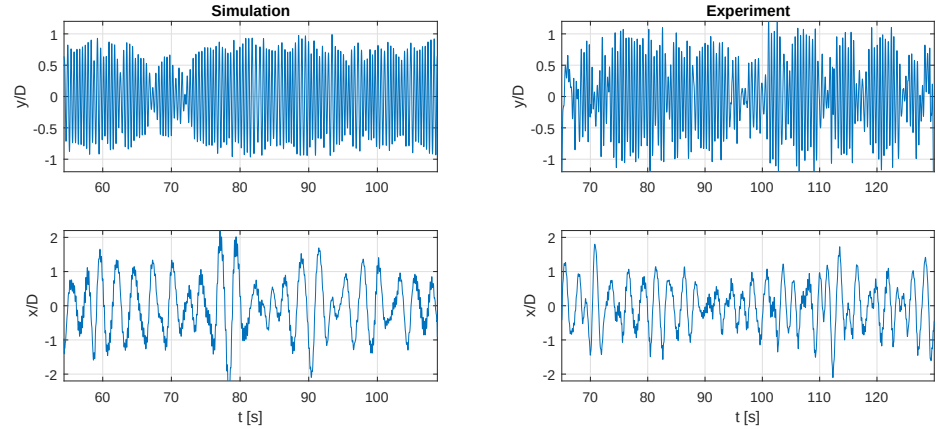


(c) $U_c = 0.282$ m/s

Figure 11: Normalized displacement time series at position of maximum rms of vibration amplitude. Case: Irregular waves + uniform current.

*VIV only*

The wave induced motion, and vibrations due to vortex shedding, are tried separated by filtering out the wave frequency components. Since the cross-flow motion does not depend strongly on the wave frequencies, the following discussions focus on the in-line part of the response. The results are presented in a similar fashion as before, i.e. dominating frequency and maximum rms of amplitude for the tested range of current velocities (figure 12), longitudinal distribution of rms of displacement and power spectra (figure 13), and displacement time series (figure 14). Pay particular attention to the power spectra in figure 13, showing (in red) frequencies that are filtered out.

From figure 12 it is seen that in-line VIV oscillate with approximately two times the cross-flow frequency, also in waves. The predictions are slightly larger than the measured frequencies, which suggests that the synchronization range (i.e. $\hat{f}_0$) could have been shifted slightly towards lower frequencies. However, it was a concious decision not to change the synchronization range, in order to demonstrate that two different flow cases could be modelled sufficiently accurate, utilizing the same set of parameters. Since the wave motion is no longer part of the response, the in-line vibration amplitudes are reduced. In this regard, the predictions agree excellent with the experiments. Looking at the longitudinal distribution of in-line amplitudes (figure 13), the response is less distributed towards the upper part of the riser, as opposed to the total in-line response. The longitudinal response variation is of a more uniform character, and resembles the results from Case 1. The displacement in-line time series in figure 14 compare well.

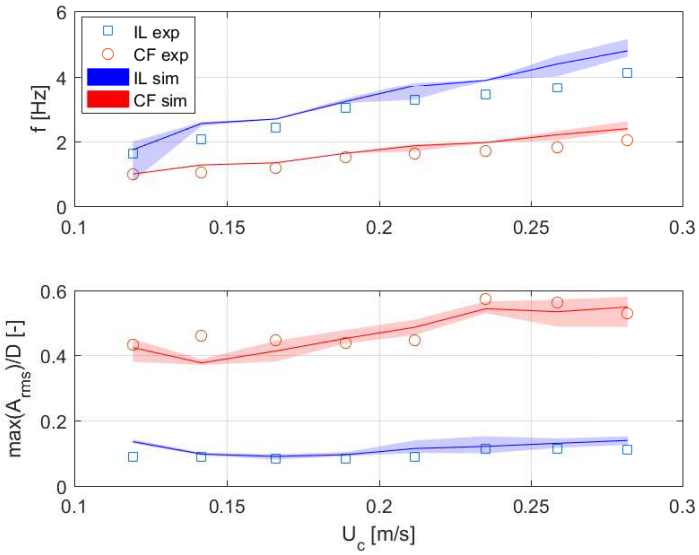


Figure 12: Upper: Dominating frequency as function of towing/current velocity. Lower: maximum rms of displacement amplitude normalized by the cylinder diameter as function of towing/current velocity. The stochastic response variation is illustrated by including envelops based on five simulations. Case: Irregular waves + uniform current, where wave frequencies have been filtered out.

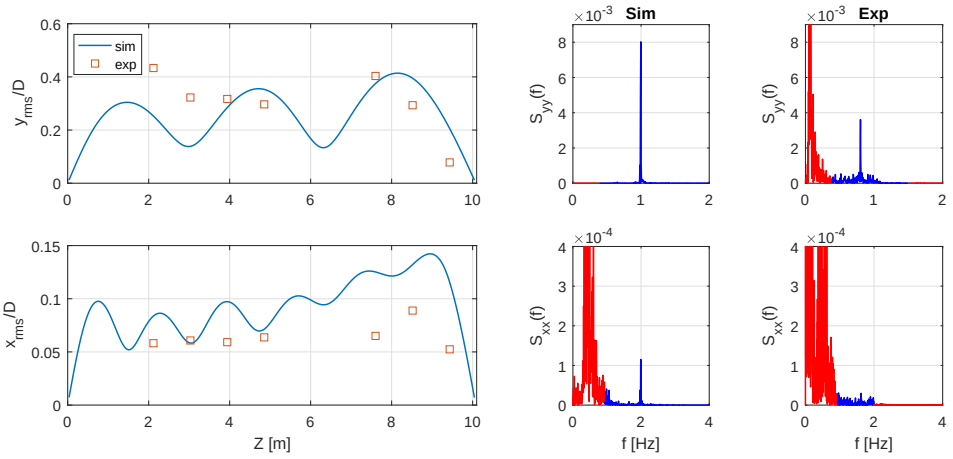


(a) $U_c = 0.119$ m/s

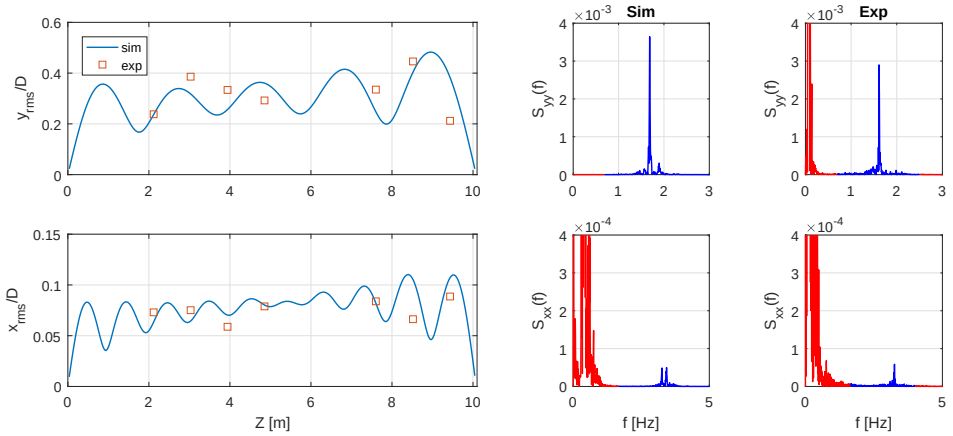


(b) $U_c = 0.212$ m/s

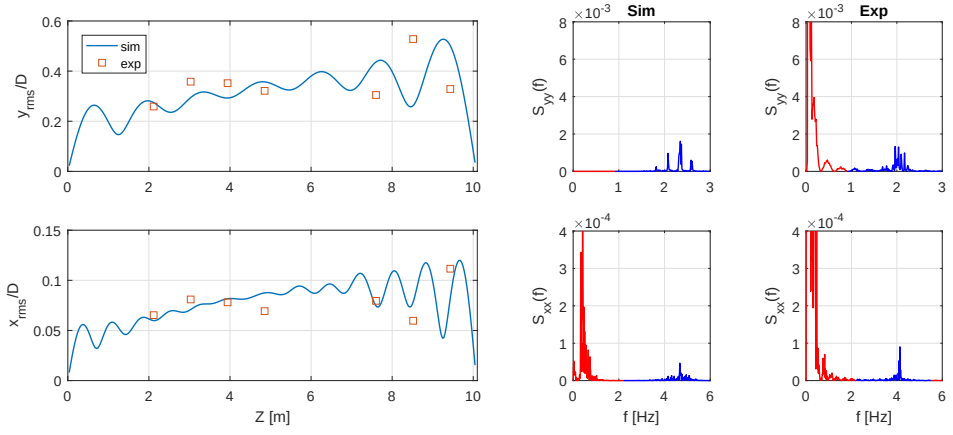


(c) $U_c = 0.282$ m/s

Figure 13: Left: Longitudinal distribution of non-dimensional displacement amplitude in terms of rms values. Right: Power spectral density of displacement at position of maximum rms value. The blue part of the power spectra illustrates the bandwidth which the presented results are based upon, and the red colour is the frequencies which have been filtered out. Case: Irregular waves + uniform current, where wave frequencies have been filtered out.

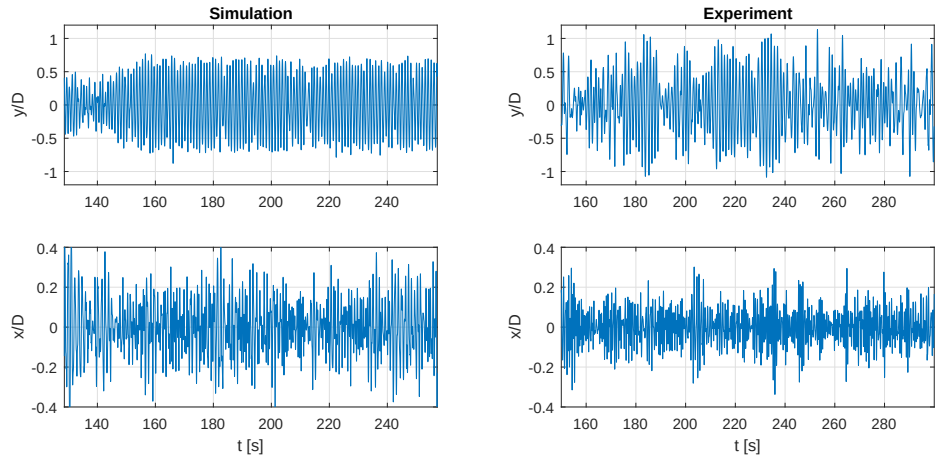


(a) $U_c = 0.119$ m/s

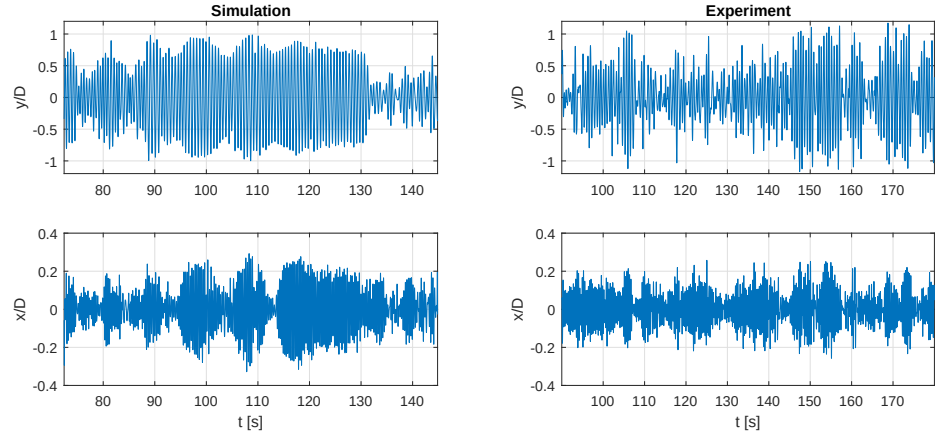


(b) $U_c = 0.212$ m/s

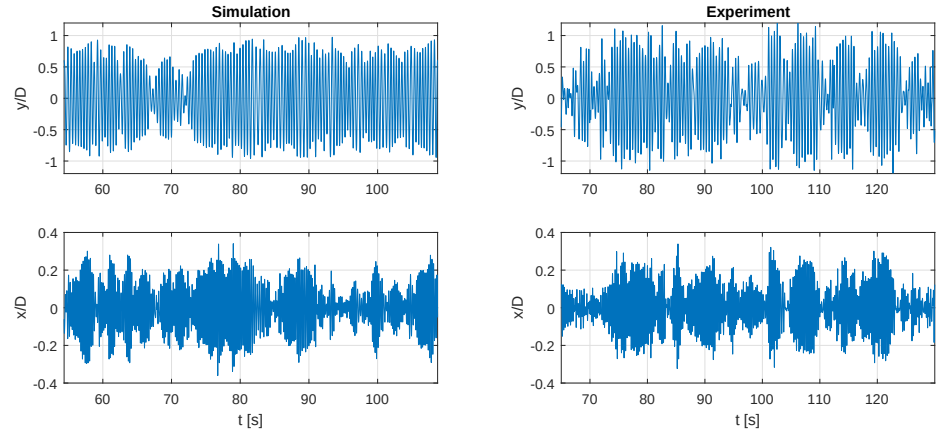


(c) $U_c = 0.282$ m/s

Figure 14: Normalized displacement time series at position of maximum rms of vibration amplitude. Case: Irregular waves + uniform current, where wave frequencies have been filtered out.

*6.4. Strain and fatigue*

Due to a low number of measurement stations along the riser, no attempt to find the experimental stain distribution is carried out. Instead, strains from simulations are calculated to compare which response type is most critical. Since there is a linear relationship between strain and stress, a study of dynamic strain amplitudes also governs the fatigue life. The output of the numerical study is presented in figure 15, showing the maximum rms of strain along the riser as function of current velocity, for the different response signals. These are: Wave, cross-flow VIV, in-line VIV and the total in-line response (containing both waves and VIV). Results for Case 1 and 2 are compared, where the former only addresses strain due to VIV (since no waves were present in the study). For Case 2, the graph represents the mean value obtained from the same five numerical simulations as before (recall figure 9 and 12).

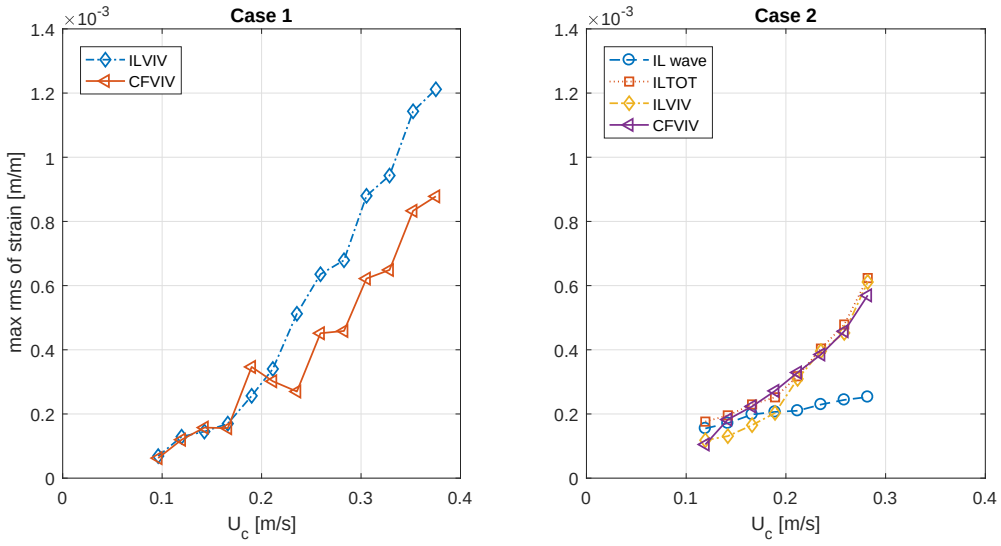


Figure 15: Comparison of maximum rms of strain due to different vibration components from simulation. These are: Waves (IL wave), in-line VIV (ILVIV), cross-flow VIV (CFVIV) and combination of in-line VIV and waves (ILTOT). Left: Case 1 (Uniform current). Right: Case 2 (Uniform current and irregular waves).

Some interesting results are noted. The maximum rms value of strain induced by the waves is only critical for the lowest values of $U_c$, roughly for $U_c < 0.15$ m/s. The wave induced strain does not vary much with the current speed, since the wave frequency and amplitude is given by the seastate only, which means that the dynamic curvature will be quite similar for all simulated velocities. This is opposed to the VIV strain signals. The vortex shedding frequency increases as the current velocity is raised, causing higher vibration modes for higher values of $U_c$. As an illustrative example, consider a standing wave type response, where the spatial distribution of in-line (or cross-flow) displacement is given by:

$$u(Z) = u_0 \sin(\frac{n\pi Z}{L}), \tag{19}$$

and $n$ is the mode of vibration. By utilizing linear beam theory, where it is assumed that plane cross-sections remain plane, the longitudinal elongation of the riser can be expressed as:

$$w(Z, x) = -x\frac{\partial u}{\partial Z}. \tag{20}$$

The most critical cross-sectional point is at the maximum obtainable value of $|x|$, which is for $x = \pm D/2$. The longitudinal engineering strain is then simply $\epsilon_{zz}(Z) = \partial w/\partial Z$. Finally, the maximum strain along the riser can be expressed as:

$$\epsilon_{zz,max} = \frac{(n\pi)^2}{2}\frac{u_0 D}{L^2}. \tag{21}$$

In words, the maximum value of strain depends on the mode of vibration squared. Hence, the reason VIV becomes more critical than the wave motion with respect to strain is that the mode of vibration, $n$, is more important than the amplitude of vibration, $u_0$ (which was significantly larger for the wave response).

Another interesting finding is how the cross-flow and in-line VIV strain signals compare. In fact, their maximum rms value follow each other quite closely for the velocity range of Case 2. However, as the current velocity is raised even more (Case 1) the in-line maximum strain seems to dominate. A similar explanation as was used to compare strain due to waves and VIV can be utilized. The cross-flow response vibrates with higher amplitudes, typically 2-3 times that of in-line VIV. However, the in-line frequency is approximately double the cross-flow vibrations, which means that the in-line response will vibrate with a higher mode. Since the bending stiffness is more or less negligible (recall table 2), it is fair to assume that the riser is tension dominated. In that case, there is a linear relationship between eigenfrequency and mode number. Roughly, this means that the in-line mode is double that of the cross-flow. As the current velocity is raised, this will become increasingly evident. It should however be noted that, as the mode number increases, the bending stiffness becomes increasingly important. Baarholm et al. [2] concluded that, in terms of fatigue, in-line VIV was governing for tensioned dominated risers, whereas cross-flow vibrations were critical in case of bending controlled risers. The conclusions were drawn based on measurements of a large scale steel riser. The transition from a tension to bending dominated system was found to match a current velocity where the dominating response mode gave equal eigenfrequency for a tensioned string and an untensioned beam.

### *6.5. VIV in different flow conditions*

It is natural to believe that vortex-induced vibrations behave differently for a riser exposed to combined current and wave action, contra current alone, due to a change in the vortex shedding process. However, the present study suggests only minor differences between the two cases, in terms of displacement amplitudes and dominating frequencies. The ratio of the experimental results for Case 1 and Case 2 (where waves are filtered out) are presented in figure 16.

Starting with the cross-flow and in-line frequencies (i.e. the two upper plots), their ratio is approximately one. Since the average inflow velocity equals $U_c$, also in case of waves, this is not particularly surprising. However, by going back to the experimental displacement power spectra (figure 6 and 13), the frequency bandwidth has not increased significantly from Case 1 to 2. This means that, even when the flow velocity varies considerably, no new frequency components are introduced in the displacement signal. It should be kept in mind that the power spectra are only representative for the displacement time series at the position of maximum rms value. But still, both for $U_c = 0.212$ m/s and 0.282 m/s, the maximum displacement rms is quite close to the mean free surface, where the effect of waves is expected to be significant. A possible explanation for why VIV is not more affected by the waves is due to the wave frequency, and the exponential decay moving downwards from the free surface. For the considered range of $U_c$, it is believed that the wave particle velocity oscillate with such a high frequency that response at a new eigenfrequency does not have time to develop before the flow acceleration again changes direction. In addition, most of the riser is (locally) unaffected by the waves. Hence, it seems that the effect of the irregular waves (on VIV) is that they mostly act as a random disturbance around the current flow.

The maximum rms value of amplitude is slightly different between the two cases. The in-line vibrations are largest for Case 1, whereas the cross-flow amplitudes, for most values of $U_c$, are slightly smaller in case of uniform current alone. The in-line results might be a consequence of having a different limit of high-pass filtering. Recall that a higher frequency limit was applied for Case 2, to remove all wave frequencies.

## 7. Conclusion

The present study has introduced a modified version of a previously published time domain force model for vortex-induced vibrations. The new approach enables time domain simulation of the response of cylindrical structures subjected to arbitrary non-stationary flow profiles, through combining a cross-flow and in-line vortex shedding force with Morison's equation. The hydrodynamic force model has been tested on an experimental case, where a vertical riser was towed with constant speed in still water and irregular waves. The numerical simulations were performed applying the hydrodynamic loads on a linear structural finite element model of the riser, and the response was found by solving the equilibrium equation with numerical time integration.

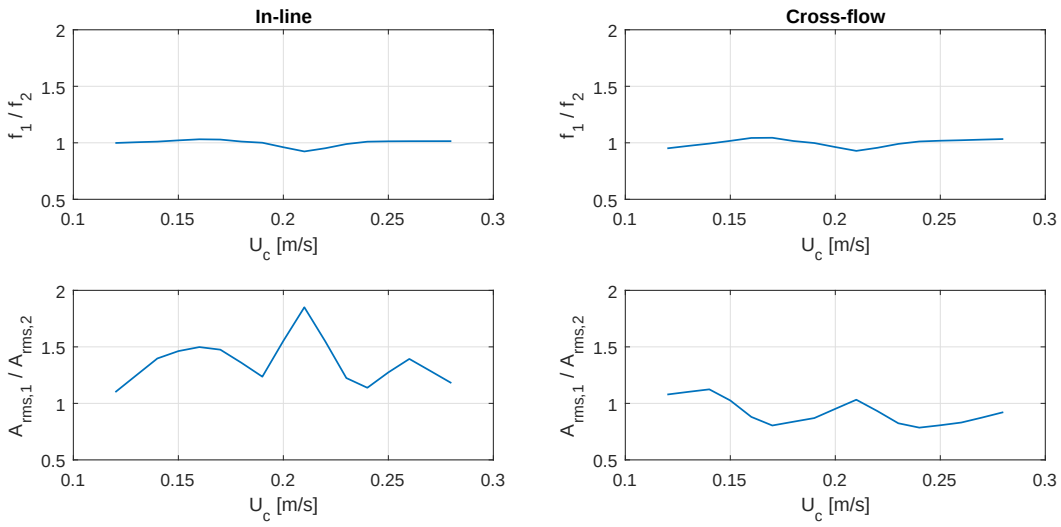


Figure 16: Ratio of experimental results between Case 1 (Uniform current) and Case 2 (Uniform current + irregular waves, for VIV frequencies only).

The case studies demonstrated good agreement between simulations and measurements in terms of displacement time series, both in cross-flow and in-line directions. In particular the case with current and irregular waves combined was predicted quite accurately. For this case, the total response (VIV+waves) and filtered signals (VIV only) were investigated separately, and the model was able to represent both situations with a high degree of realism. Maximum rms of strain was then calculated from the numerical simulations, for the different response components separately (i.e. wave, in-line VIV, cross-flow VIV and wave+in-line VIV). The output showed that strain induced by waves was only ciritcal for very low current speeds. As the latter was raised, VIV became increasingly important despite lower amplitudes, due to higher modes of vibration. The strains from cross-flow and in-line vortex-induced vibrations were of comparable size. Finally, the riser response due to current alone, and the combined load from current and waves, was compared, applying the experimental time series. It was concluded that displacements due to VIV were very similar for the two flow cases. The resemblance was assumed to raise from the combination of high wave frequencies, and the fact that the waves decay exponentially downwards from the free surface.

The convincing performance of the numerical model illustrates its future potential as an engineering tool for analysis of slender marine structures subjected to waves and current. The state of the art procedure, using Morison's equation alone, can easily be replaced by adding the two vortex shedding terms. A few new empirical parameters are introduced, but, as demonstrated by applying the same coefficients for the two different flow cases, they can be quantified quite generally. In the end, the advantage is that the effect of vortex shedding can apparently be modelled even in quite complex flows, in combination with other hydrodynamic load effects predicted by Morison's equation. Further work should investigate what happens if waves and current come from different directions, and how accumulated fatigue damage compare when wave and VIV analyses are performed separately versus combined.

## 8. Acknowledgement

Norwegian Deepwater Programme (NDP) are acknowledged for providing and allowing their experimental data to be published.

## 9. References

[1] Aronsen, K. H., 2007. An Experimental Investigation of In-line and Combined In-line and Cross-flow Vortex Induced Vibrations. Ph.D. thesis, Norwegian University of Science and Technology (NTNU).

[2] Baarholm, G., Larsen, C., Lie, H., 2006. On fatigue damage accumulation from in-line and cross-flow vortex-induced vibrations on risers. Journal of Fluids and Structures 22 (1), 109–127.

[3] Blevins, R. D., Coughran, C. S., 2009. Experimental Investigation of Vortex-Induced Vibration in One and Two Dimensions With Variable Mass, Damping, and Reynolds Number. J. Fluids Eng. 131 (October 2009), 101202.

[4] Chang, S., Isherwood, M., 2003. Vortex-Induced Vibrations of Steel Catenary Risers and Steel Offloading Lines due to Platform Heave Motions. In: Offshore Technology Conference.

[5] Dahl, J. M., Hover, F. S., Triantafyllou, M. S., Oakley, O. H., 2010. Dual resonance in vortex-induced vibrations at subcritical and supercritical Reynolds numbers. Journal of Fluid Mechanics 643, 395–424.

[6] Faltinsen, O., 1990. Sea loads on ships and offshore structures. Cambridge University Press.

[7] Fu, S., Wang, J., Baarholm, R., Wu, J., Larsen, C. M., 2014. Features of Vortex-Induced Vibration in Oscillatory Flow. Journal of Offshore Mechanics and Arctic Engineering 136.

[8] Kaasen, K. E., Lie, H., Solaas, F., Vandiver, J. K., 2000. Norwegian Deepwater Program: Analysis of Vortex-Induced Vibrations of Marine Risers Based on Full-Scale Measurements. In: Offshore Technology Conference.

[9] Kozakiewicz, A., Sumer, B. M., Fredsøe, J., 1994. Cross-Flow Vibrations of Cylinder in Irregular Oscillatory Flow. Journal of Waterway, Port, Coastal, and Ocean Engineering 120 (6), 515–534.

[10] Liao, J.-C., 2001. Vortex-induced Vibration of Slender Structures in Unsteady Flow. Ph.D. thesis, Massachusetts Institute of Technology.

[11] Mo, K., 1999. Vortex induced vibrations of a riser with forced motions. Model tests in current and in waves. Tech. rep., Norwegian Marine Technology Research Institute.

[12] Passano, E., Larsen, C. M., Lie, H., Wu, J., 2014. Vivana Theory Manual. Tech. rep.

[13] Resvanis, T. L., 2014. Vortex-Induced Vibration of Flexible Cylinders in Time-Varying Flows. Ph.D. thesis, Massachusetts Institute of Technology.

[14] Sarpkaya, T., may 2004. A critical review of the intrinsic nature of vortex-induced vibrations. Journal of Fluids and Structures 19 (4), 389–447.

[15] Sumer, B. M., Fredsøe, J., 1988. Transverse Vibrations of an Elastically Mounted Cylinder Exposed to an Oscillating Flow. Journal of Offshore Mechanics and Arctic Engineering 110 (November 1988), 387–394.

[16] Sumer, B. M., Fredsoe, J., 2006. Hydrodynamics Around Cylindrical Structures, Revised Edition. World Scientific Publishing Co. Pte. Ltd.

[17] Thorsen, M., Sævik, S., Larsen, C., 2014. A simplified method for time domain simulation of cross-flow vortex-induced vibrations. Journal of Fluids and Structures 49, 135–148.

[18] Thorsen, M., Sævik, S., Larsen, C., feb 2016. Time domain simulation of vortex-induced vibrations in stationary and oscillating flows. Journal of Fluids and Structures 61, 1–19.

[19] Thorsen, M., Sævik, S., Larsen, C., 2017. Non-linear time domain analysis of cross-flow vortex-induced vibrations. Marine Structures 51, 134–151.

[20] Thorsen, M. J., Sævik, S., 2017. Simulating riser VIV in current and waves using an empirical time domain model. In: Proceeding of the ASME 2017 36th International Conference on Ocean, Offshore and Arctic Engineering.

[21] Thorsen, M. J., Sævik, S., Larsen, C. M., 2015. Fatigue damage from time domain simulation of combined in-line and cross-flow vortex-induced vibrations. Marine Structures 41, 200–222.

[22] Thorsen, M. J., Sævik, S., Larsen, C. M., 2015. Time Domain Simulation of Vortex-Induced Vibrations Based on Phase-Coupled Oscillator Synchronization. In: ASME 2015 34th International Conference on Ocean, Offshore and Arctic Engineering.

[23] Ulveseter, J., Sævik, S., Larsen, C., 2017. Time domain model for calculation of pure in-line vortex-induced vibrations. Journal of Fluids and Structures 68, 158–173.

[24] Ulveseter, J. V., Sævik, S., 2017. In-line vibrations of flexible pipes. In: Proceedings of the ASME 2017 36th International Conference on Ocean, Offshore and Arctic Engineering.

[25] Vandiver, J. K., Jaiswal, V., Swithenbank, S. B., Jhingran, V., 2006. Fatigue damage from high mode number vortex-induced vibration. In: Proceedings of the 25th International Conference on Offshore Mechanics and Arctic Engineering.

[26] Vandiver, J. K., Li, L., 2005. SHEAR7 V4.4 Program Theoretical Manual. Tech. rep., Department of Ocean Engineering Massachusetts Institute of Technology.

[27] Wang, J., Fu, S., Baarholm, R., Wu, J., Larsen, C. M., 2014. Fatigue damage of a steel catenary riser from vortex-induced vibration caused by vessel motions. Marine Structures 39, 131–156.

[28] Williamson, C., Govardhan, R., 2008. A brief review of recent results in vortex-induced vibrations. Journal of Wind Engineering and Industrial Aerodynamics 96 (6), 713–735.

[29] Zhao, M., Pearcey, T., Cheng, L., Xiang, Y., 2017. Three-Dimensional Numerical Simulations of Vortex-Induced Vibrations of a Circular Cylinder in Oscillatory Flow. Journal of Waterway, Port, Coastal, and Ocean Engineering.